Construction and Building Materials 335 (2022) 127485

Contents lists available at ScienceDirect

Construction and Building Materials

journal homepage: www.elsevier.com/locate/conbuildmat

Influence of non-linear soil properties on railway critical speed

Jesus Fernández-Ruiz [a,*], Alexandre Castanheira-Pinto [b], Pedro Alves Costa [b], David P. Connolly [c]

[a] Universidade da Coruña, Departamento de Ingeniería Civil, Campus de Elviña, s/n, A Coruña, Spain
[b] Construct-FEUP, University of Porto, Porto, Portugal
[c] School of Civil Engineering, University of Leeds, Leeds, UK

ARTICLE INFO

Keywords:
Railway critical speed
Soil stiffness non-linearity
High-speed railways
Plasticity index
Railway dynamics

ABSTRACT

The design of high-speed railway lines involves geotechnical challenges, one of which is the risk of dynamic track amplification, for example on track sections where the train speed approaches the track-ground critical speed. In these cases, soil strains increase significantly with an increase in train speed, far exceeding the limits of linear elastic behaviour. This can result in a non-linear reduction of soil stiffness. To better understand this relationship, this paper studies the influence of soil non-linearity on the critical speed of concrete slab and ballasted tracks. To perform an in-depth analysis into non-linear critical speed, two models are used: a 3D FEM approach, and a novel dispersion curve technique. Using the models, the effect of soil plasticity on non-linearity is studied, with different ranges of plasticity found to play an important role. Secondly, the influence of soil thickness and loading magnitude are evaluated. It is shown that ballasted tracks are deeply affected by the non-linear soil behaviour, compared to a concrete slab track. Further, it is shown that for the ballasted tracks, the relationship between the critical speed and shallow upper soil layer thickness can be weak.

1. Introduction

During the last few decades there has been a significant growth in the development of high-speed railway lines, mainly due to the advantages they offer in terms of travel time and sustainability.

From a geotechnical point of view, there are several challenges in the design and implementation of high-speed railway lines [1,2]. One of these is the presence of soft soils, characterised by low wave propagation speeds ($C_s < 100$–120 m/s), in which dynamic wave propagation can be induced, as the speed of the train (≈ 80–90 m/s) approaches the natural wave speeds in the track and ground materials. This phenomenon is well known in railway geotechnical engineering and it is called "critical speed" [3–6], which formally corresponds to the speed of a non-oscillating moving load that causes the largest amplification of the dynamic response of the track [7]. When this occurs, there is an increase in the deformations of the ballast and subgrade, increasing the risk of derailment [8] and maintenance costs.

In recent years, the scientific community has taken steps towards a deeper knowledge and understanding of the critical speed phenomenon. Since the 2000 s, when the Ledsgard case marked the beginning of the study of this phenomenon [9–14], different methods have been proposed for calculating the critical speed, ranging from analytical solutions [3–6,15,16] to numerical models. Among these it is worth highlighting the 2.5D numerical approaches [4,17–20], especially suitable for homogeneous geometries in the longitudinal direction of the track, and periodic numerical models [21,22], suitable for simulating periodic structures in the longitudinal direction of the track, both formulated in the frequency/wavenumber domain.

When the geometry is neither homogeneous nor periodic, 3D numerical models are typically required [23]. These can be formulated in the frequency domain, for example using boundary elements to prevent wave reflections [24–26]; or in the time domain, which tend to be more demanding in terms of computational efficiency, but more versatile for the study of complex geometries and non-linear behaviour [27–32].

When the train approaches the critical speed of the track-ground system, soil strains are amplified and the strain range can exceed the linear elastic threshold. Although in most of the researches on critical speed the linear elastic model has been used to simulate the behaviour of the soil, in recent years a few studies have been presented on the influence of non-linear soil behaviour, both by means of the linear equivalent approach [14,27,33] and with truly non-linear models [27,28]. Abu Sayeed and Shahin [28] showed how the non-linear behaviour of the soil has limited little influence on the critical speed on ballast tracks. However, Dong et al. [33], through a linear equivalent

* Corresponding author.
E-mail address: jesus.fernandez.ruiz@udc.es (J. Fernández-Ruiz).

https://doi.org/10.1016/j.conbuildmat.2022.127485
Received 16 February 2022; Received in revised form 29 March 2022; Accepted 10 April 2022
Available online 19 April 2022

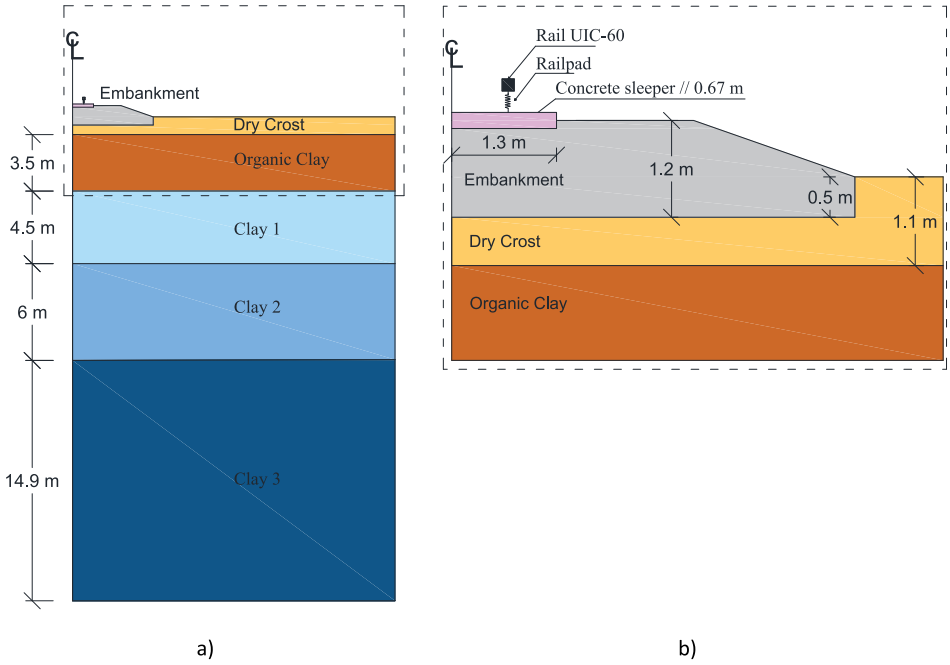

Fig. 1. Ledsgard characteristics: a) global view; b) detailed view.

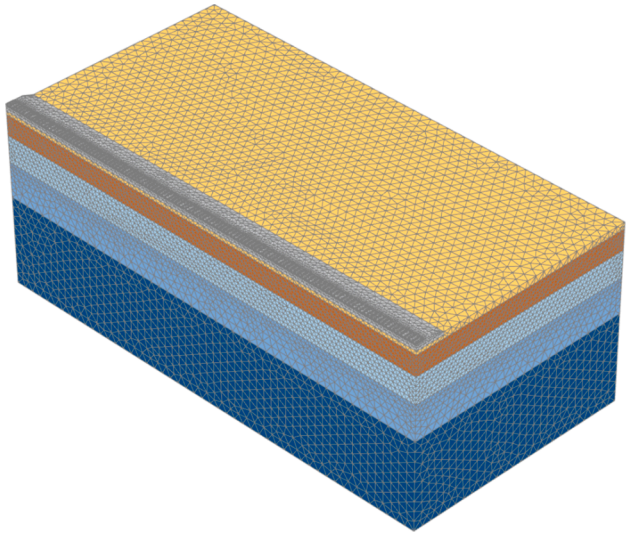

Fig. 2. Finite element mesh of Ledsgard case.

approach, showed how the non-linear behaviour of the soil has a relevant effect on the critical speed for ballast tracks, causing a reduction in the critical speed of between 11% and 20% with respect to the linear elastic assumption. Also, Alves Costa et al [14] and Shih et al. [27] found that the critical speed is significantly lower when linear equivalent models and non-linear models are used to simulate the behaviour of railway subgrade.

The linear equivalent approach and, in general, most non-linear soil models, are based on the stiffness and damping curves as a function of cyclic strain. These curves are influenced by several geotechnical parameters such as: mean principal effective stress (p'), plasticity index (PI), void ratio (e), over-consolidation ratio (OCR) and the number of cycles [34–36]; with PI and p' being the most influential values [37]. According to Ishibashi and Zhang [38] the effect of p' is more important for soils with PI values lower than 15–30, while for higher PIs its effect is negligible. Regarding the effect of PI, Vucetic and Dobry [37] concluded that soils with a high plasticity tend to exhibit a more linear behaviour at small strain compared to soils with a lower PI.

In this context, the main objective of this research is to undertake a thorough numerical analysis of the influence of soil non-linearity on the critical speed of high-speed railway lines, considering both slab and ballasted track. The novel contributions are the analysis of PI and soft soil thickness on critical speed. In particular, the influence of the load magnitude on critical speed is studied, considering both types of tracks and different values of PI.

2. Numerical modelling

In this section, the dynamic response of railway track foundations to moving loads is experimentally validated using a non-linear soil model. For this, a well-documented case in the technical literature, Ledsgard [14], is used.

2.1. Numerical model description

The numerical model is a 3D FEM model formulated in the time domain, developed using Plaxis software [39]. The geotechnical profile of Ledsgard [14] and the numerical model are shown in Fig. 1 and in Fig. 2. The dimensions of the model are 80x40x30 m in the longitudinal, horizontal and vertical directions respectively, thus making the domain similar in dimensions to the values used in alternative 3D models of the same site [29,31,40–42]. The railpad is modelled as a linear spring **($k_p = 250{\cdot}10^6$ N/m and $c_p = 22.5{\cdot}10^3$ N·s/m)**, whereas the rail is simulated as a beam, equivalent to a UIC-60 section. The remaining track components (sleeper, ballast and subballast) and ground are modelled using 3D solid elements.

The numerical model is made up of 370,181 elements and 523,961 nodes **with an average element size of 1.231 m. The maximum element size is 3.863 m and the minimum size is 0.066069 m.** Quadratic tetrahedral solid elements (10 node elements) are used. To prevent boundary reflections, viscous dampers [39] are applied on domain edges, except in the symmetry plane, where the horizontal movements are impeded.

Regarding the numerical modelling of moving loads, this is applied using the equivalent nodal force method, in keeping with that stated in

Table 1
Soil elastic properties.

Layer	h (m)	ρ (kN/m^3)	G_0 (kN/m^2)	ν (-)
Embankment	1.2	18.00	79.51×10^3	0.19
Dry crust	1.1	15.00	5.95×10^3	0.49
Organic Clay	3.5	12.60	2.17×10^3	0.49
Clay 1	4.5	14.75	5.31×10^3	0.49
Clay 2	6	14.75	11.18×10^3	0.49
Clay 3	14.9	14.75	14.75×10^3	0.49

where h makes reference to the soil thickness, ρ the soil density and ν to Poisson's ration.

[43]. **For this purpose, the train moving load is considered as triangular pulse distributed along three nodes, as described in [28]. In this context**, the time interval is defined according to the Courant-Friedrichs-Lewy criteria [27,28], with an implicit Newmark integration scheme, as shown below:

$$C_n = \frac{\Delta t \times c}{L_{\min}} < 1 \tag{1}$$

where: C_n is the Courant number, Δt is the time interval, c is the speed of the moving load and $L_{\min}$ is the distance between two adjacent loading nodes. **In all models, the Courant number was assumed 0.95.**

2.2. Soil constitutive model

The constitutive model to simulate the non-linear behaviour of the soil is the Hardening Soil Small Strain Model [44,45], which is a soil model that takes into account the G degradation curve as function of the soil strain. The Mohr-Coulomb failure criterion is used and the model is capable of simulating both shear and compression soil hardening, using hyperbolic laws combined with classical plasticity theory. For unloading–reloading cycles, the model follows the Masing rules, also showing hysteretic damping [44].

As regards the degradation curves of G and the damping considered in the HSsmall model, these have the following equations [46]:

$$G_s/G_0 = \frac{1}{1+\frac{0.385\cdot\gamma}{\gamma_{0.7}}} \tag{2}$$

$$\xi = \frac{E_D}{4\pi E_s} \tag{3}$$

$$E_D = \frac{4G_0\cdot\gamma_{0.7}}{0.385}\left(2\cdot\gamma - \frac{\gamma}{1+\gamma_{0.7}/0.385\cdot\gamma} - \frac{2\cdot\gamma_{0.7}}{0.385}\cdot\ln\left(1+\frac{0.385\cdot\gamma}{\gamma_{0.7}}\right)\right) \tag{4}$$

$$E_s = \frac{G_0\cdot\gamma^2}{2+2\cdot0.385\cdot\gamma/\gamma_{0.7}} \tag{5}$$

where **E_D is the area of the closed loop, E_S is the energy stored at maximum strain γ_{max},** G_0 is the small strain shear stiffness, G_s is the secant shear stiffness, γ is the shear strain, $\gamma_{0.7}$ is the shear strain for $G_s/G_0 = 0.722$ and ξ is the damping.

The geotechnical properties at Ledsgard are shown in Table 1 and Table 2, in accordance with that shown by Alves Costa et al. [14].

Fig. 3 shows the degradation curve of G and the damping.

2.3. Experimental validation

For the validation of the constitutive model of the soil, the results are compared with real measurements [14]. Four different train speeds are considered: 70, 140, 180 and 204 km/h. The mechanical and geometric characteristics of the train are shown in Alves Costa et al. [14].

Fig. 4 shows the results for each speed, showing a good fit for all cases, both for speeds lower than the critical speed (70–140 km/h) and those closer to the critical speed (180–204 km/h). Although

Table 2
Soil properties in HSsmall model.

Layer	E_{50} (kN/m^2)	E_{oed} (kN/m^2)	E_{ur} (kN/m^2)	φ (°)	C (kN/m^2)	Ψ (°)
Embankment	16.67×10^3	16.67×10^3	35.00×10^3	45.00	5.00	12.00
Dry crust	0.75×10^3	0.75×10^3	2.25×10^3	0.00	50.00	0.00
Organic Clay	0.40×10^3	0.40×10^3	1.20×10^3	0.00	30.00	0.00
Clay 1	0.70×10^3	0.70×10^3	2.10×10^3	0.00	30.00	0.00
Clay 2	1.37×10^3	1.37×10^3	4.12×10^3	0.00	40.00	0.00
Clay 3	1.62×10^3	1.62×10^3	4.87×10^3	0.00	50.00	0.00

where E_{50} is the secant Young modulus for stress level corresponding to 50% of the shear strength, E_{oed} is the oedometric Young modulus, E_{ur} is the unloading–reloading stiffness and Ψ the dilatancy angle.

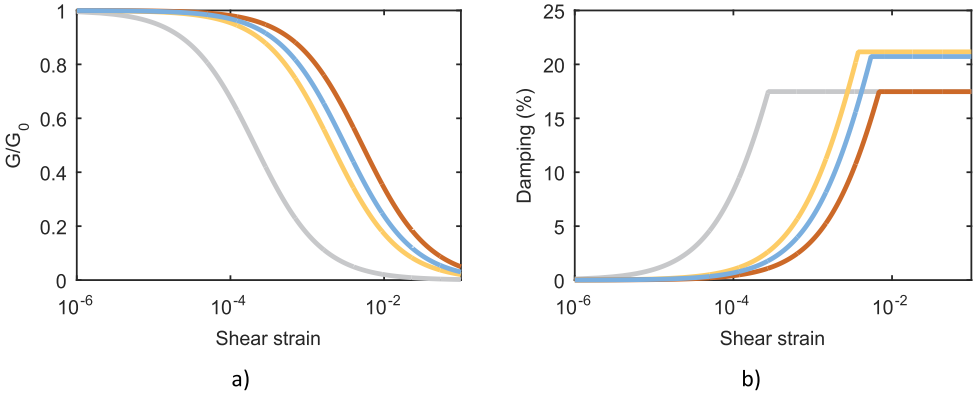

Fig. 3. Degradation curves for: a) shear modulus reduction; b) Damping ratio (grey colour – embankment; yellow colour – dry crust; brown colour – organic clay; blue colour – clay 1, 2 and 3).

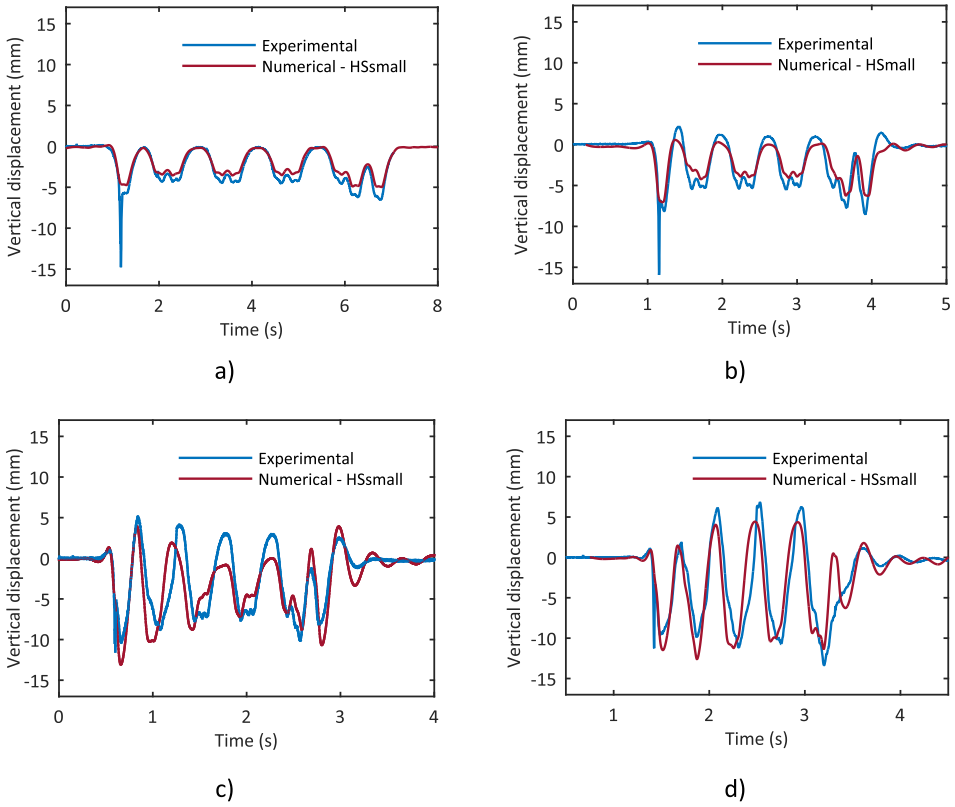

Fig. 4. Comparison between computed time histories of sleeper displacements for different train speeds (Southbound direction): (a) V = 70 km/h; (b) 140 km/h; (c) V = 180 km/h and (d) V = 204 km/h.

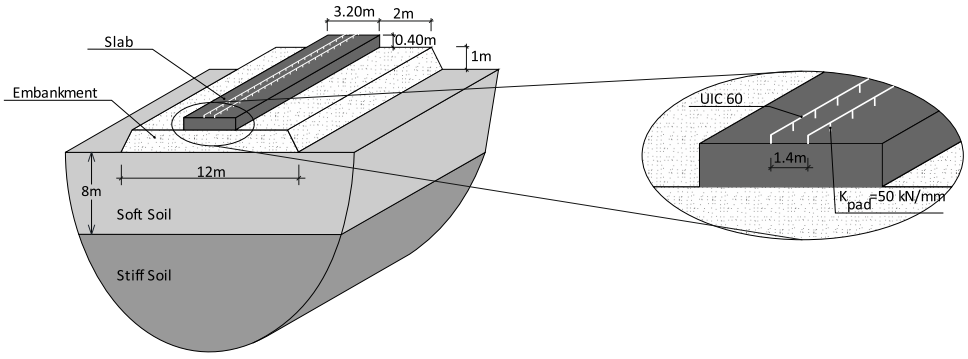

Fig. 5. Reference case for the concrete slab track.

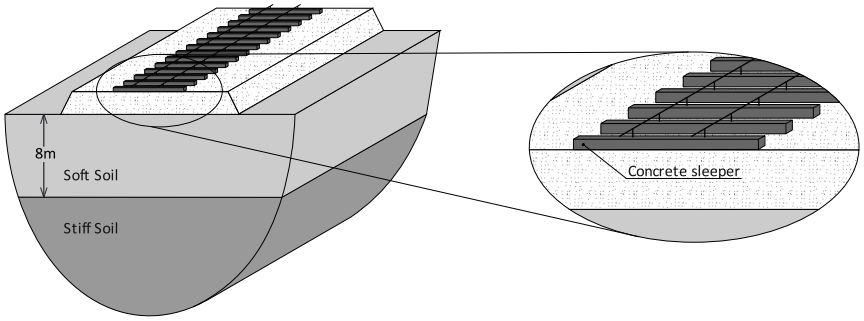

Fig. 6. Reference case for the ballast track.

Table 3
Material properties.

Layer	E (MPa)	ρ (Kg/m^3)	ν (-)	ξ (-)	C_s (m/s)
Slab/Sleeper	25e3	2500	0.20	0.01	**2041**
Embankment (ballast and subballast)	200	2000	0.30	0.03	196
Soft soil	30.5	1600	0.35	0.03	**84**
Stiff soil	208	2000	0.30	0.03	200
Rail (UIC 60)	210e3	7850	0.30	0.01	**3208**
Rail pads	**$K_{pad} = 50{\cdot}10^6$N/m, $C_p = 22.5{\cdot}10^3$N·s/m and 0.6 m of longitudinal spacing**				

some discrepancies are shown, overall a strong agreement in terms of shape and magnitude is found. Therefore, the model is considered acceptable for studying the response of alternative high-speed railway lines, where the non-linear behaviour of the soil plays a relevant role.

3. Influence of plasticity index (PI)

3.1. Reference scenario

An objective of this study is to evaluate the influence of non-linear soil behaviour on the track-ground critical speed. To enable a comparison of the effects of linear versus non-linear behaviour, a linear reference case for both ballast and concrete slab track is defined. This then allows for different non-linear parameters to be compared against a benchmark. Thus, Fig. 5 and Fig. 6 show the reference cases for the slab and ballasted tracks respectively. The corresponding linear elastic material properties are shown in Table 3.

The critical speed for the reference scenario is computed using Plaxis 3D. The dynamic amplification factor (DAF) and vertical displacement field at the critical speed are presented in Fig. 7 for the slab track, and in Fig. 8. for the ballasted track. As can be seen, the critical speed for the ballasted track is considerably smaller compared to the slab. This is because ballasted tracks have reduced bending stiffness, and therefore sensitive to the geotechnical properties of the shallow soil, in

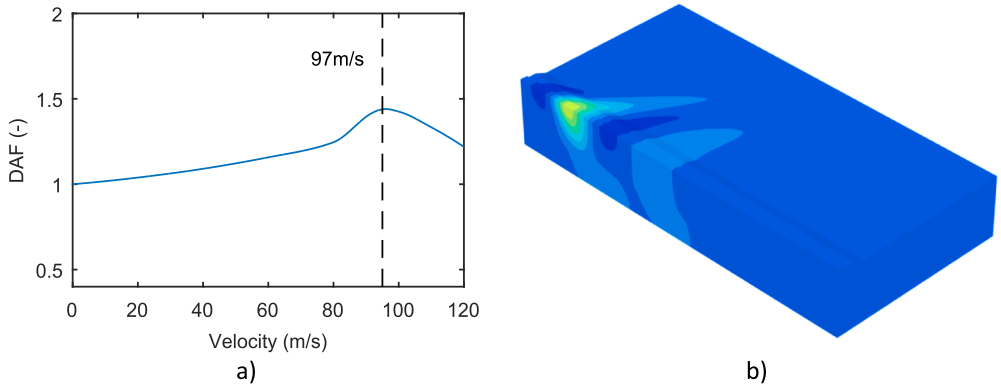

Fig. 7. Results for the slab track reference case: a) DAF curve; b) vertical displacement field at the critical speed.

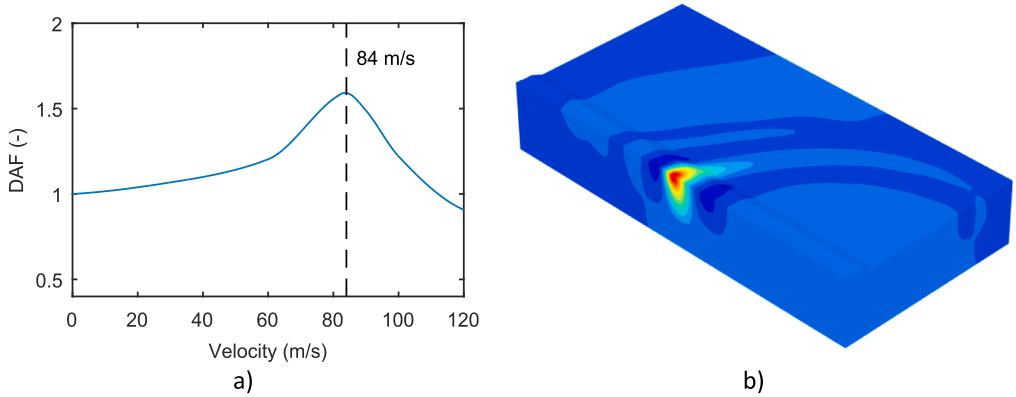

Fig. 8. Results for the ballast track reference case: a) DAF curve; b) vertical displacement field at the critical speed.

Table 4
Material properties adopted for the HSsmall model.

Element	E_{50} (kN/m^2)	E_{oed} (kN/m^2)	E_{ur} (kN/m^2)	φ (°)	c (kN/m^2)	Ψ (°)	$\gamma_{0.7}$
Embankment (ballast and subballast) (PI 0)	35×10^3	35×10^3	70×10^3	45	5	10	7.5×10^{-5}
Soft soil (PI 70)	1.3×10^3	1.3×10^3	4×10^3	0	50	0	1.4×10^{-3}
Soft soil (PI 50)	1.3×10^3	1.3×10^3	4×10^3	0	50	0	9.7×10^{-4}
Soft soil (PI 30)	1.3×10^3	1.3×10^3	4×10^3	0	50	0	6.7×10^{-4}
Soft soil (PI 15)	1.3×10^3	1.3×10^3	4×10^3	0	50	0	3.6×10^{-4}
Stiff soil	40×10^3	40×10^3	80×10^3	35	5	10	2.4×10^{-4}

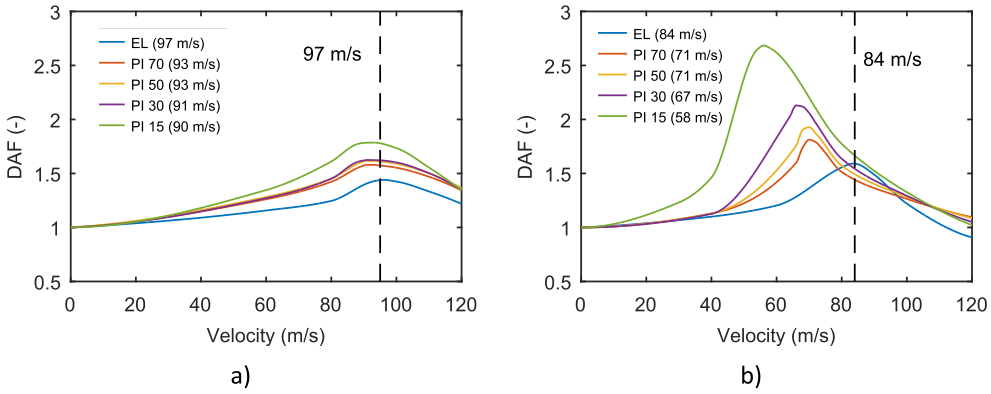

Fig. 9. DAF curves for different plasticity index: a) slab track; b) ballasted track.

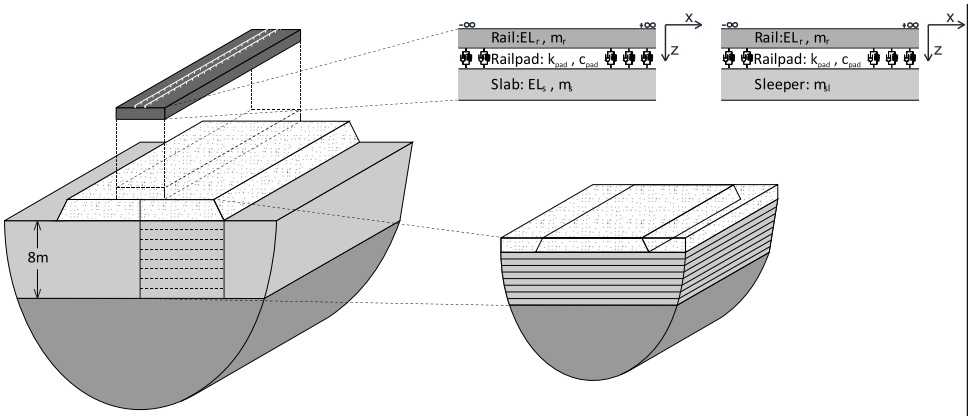

Fig. 10. Schematic illustration of how the real section is translated in the analytical model.

comparison to slab tracks. Another interesting aspect that should be highlighted is the magnitude and shape of the displacement field at the critical speed. The Fig. 7 and Fig. 8 show that the ballast track develops greater displacement, thus leading to higher amplification.

3.2. Non-linear approach

To study the influence of nonlinear soil properties on the critical speed, four scenarios are analysed. These have similar properties to the reference cases, however the soil has varying plasticity indexes: 15, 30, 50 and 70, **which generally characterise the range values of plastic soils** [47]. All scenarios consider the Hardening Soil Small (HSsmall) constitutive model to describe the mechanical behaviour of the soils, as well as for the embankment. It should be mentioned that the authors assumed the embankment as a composed layer of ballast and suballast. Table 4 shows the material properties used as inputs for the HSsmall.

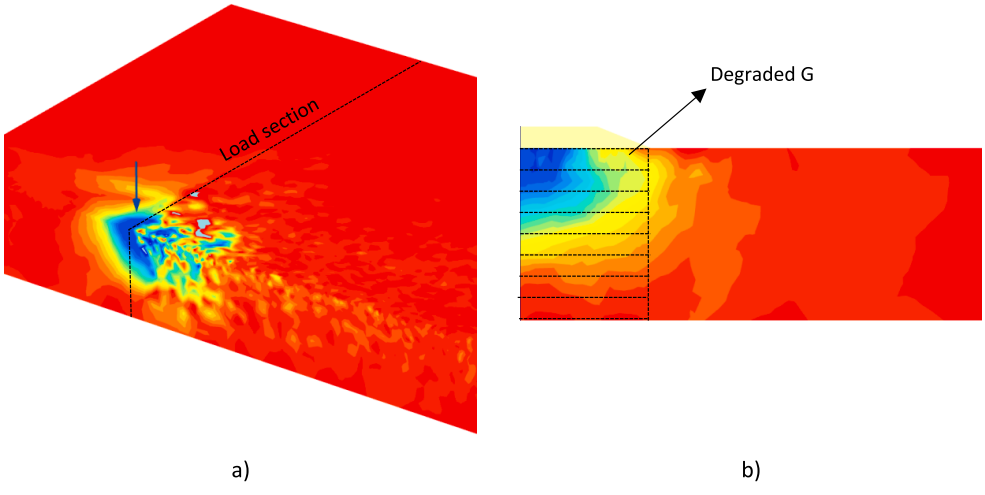

Fig. 11. Spatial G degradation or PI 70 slab track: a) 3D view; b) Cross section on the loading plane.

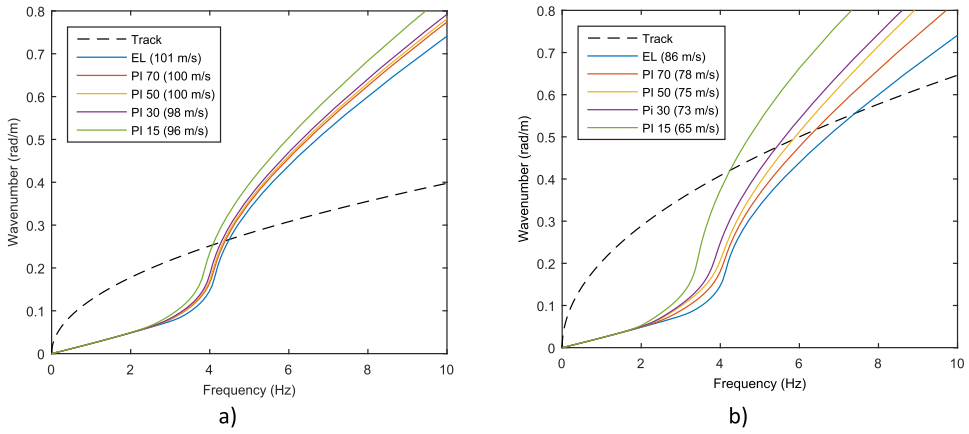

Fig. 12. Dispersion curves for all PI assumed: a) slab track; b) ballasted track.

The $\gamma_{0.7}$ values are considered according to the suggestion presented by Ishibashi and Zhang [36]. It should be pointed out that for the soft soil, only the $\gamma_{0.7}$ value is altered for the different PIs considered, while the remaining parameters are kept constant. Typically, the stiffness of a soil is lower if the PI is high, however, the Norwegian Geotechnical Institute [47] has tested clays with C_s values between 80 and 100 m/s and yet PI variables between 10 and 53. Hence, although less common, it is possible to find clays with low C_s values but high PIs.

The critical speed is computed, considering an axle load of 180kN [17], for the range of PI (plasticity index) values, with the results summarized in Fig. 9a for slab track and in Fig. 9b for ballasted track. Firstly, as can be observed, allowing non-linearity to develop gives rise to lower critical speeds in comparison to the linear elastic case, which is due to the degradation of soil stiffness. Further, for lower PIs, higher levels of degradation are induced, and consequently, the critical speed is lower. Nevertheless, the differences found between both track systems are meaningful, showing that the critical speed in slab tracks is reduced by between 3 and 8% in comparison with the linear elastic case. Additionally, the effect of soil non-linearity is more pronounced in ballasted tracks, where the differences are up to the magnitude of 30%.

In order to further investigate the influence of PI on the critical speed, an analytical procedure, where the critical speed is computed using dispersive analysis [4,48], is also used. For this, both the track and the soil media are described analytically (the mathematical approach followed is described in APPENDIX). Fig. 10 shows a schematic illustration of how both systems are considered for the dispersive analysis, where it can be seen that the slab track is modelled as a two-layered Bernoulli-Euler beam connected with springs and dashpots. For ballasted track, the system is similar but considers the sleepers as a beam without bending stiffness. Regarding the soil stratum, the average degraded soil properties are computed using Plaxis 3D. Vertically the soil is divided into horizontal layers with one meter thickness, whereas horizontally the region is limited by the embankment, as shown in Fig. 10. This makes it possible to include the degradation produced by nonlinear behaviour in the analytical analysis.

To better illustrate the procedure followed, a detailed explanation is now presented. To evaluate the resulting properties, a transversal section on the loading plane, as shown in Fig. 11a, is considered. For that section, the average G modulus is computed for an area beneath the embankment (Fig. 11b). To better discretized the degradation obtained the authors suggest to divide the soil into 1 m thickness layers, as shown in Fig. 11b.

With the degradation obtained for each of the soil layers it can be computed the reduced linear properties using the following equation:

$$c_d = \sqrt{G/G_0}\cdot c \tag{2}$$

where c_d is the degraded wave velocity, G/G_0 the degradation obtained and c the linear wave velocity.

Fig. 12 shows the dispersion curves obtained considering the degradation pattern for the soil for all the cases expressed in Fig. 9. Note that the critical speed is determined using the intersection point of the track and ground dispersion curves [4,48,49]. As can be seen in Fig. 12a, for slab tracks the intersection point occurs on a branch of the soil dispersion curve where the degradation pattern does not have a great

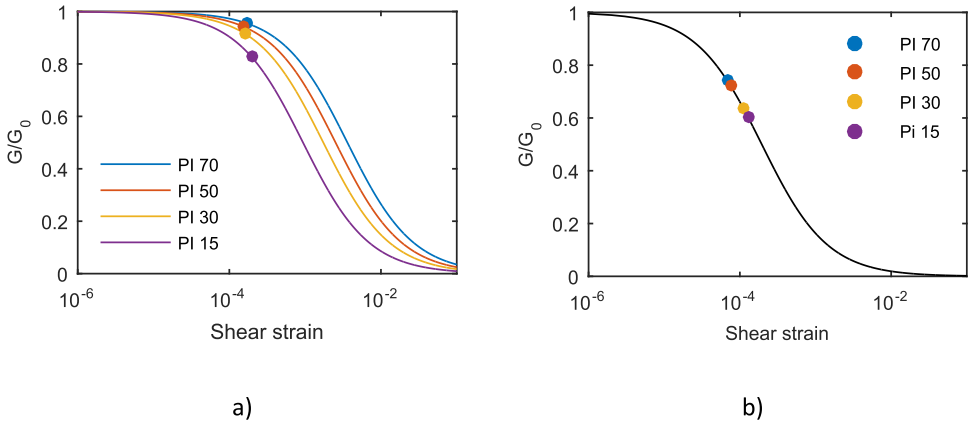

Fig. 13. Average G-degradation in slab track: a) soil; b) embankment.

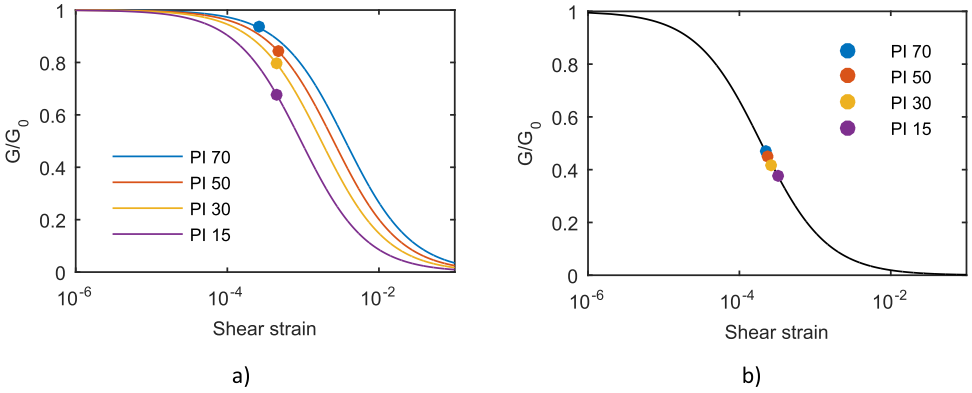

Fig. 14. Average G-degradation in ballasted track: a) soil; b) embankment.

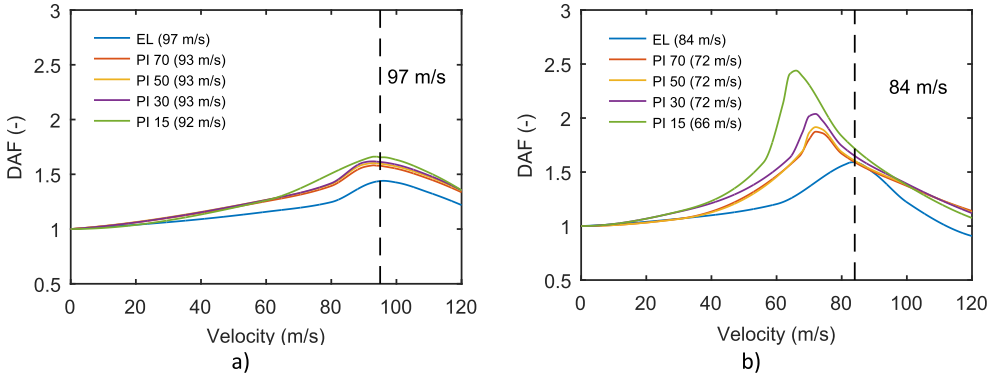

Fig. 15. DAF curves for an axle load of 120 kN: a) slab track; b) ballasted track.

influence. This fact can be explained by taking into consideration that lower frequencies are associated with higher wavelengths, and, consequently, are less sensitive to local characteristics, such as stiffness degradation at shallow depth. In contrast, the ballasted track dispersion curve (Fig. 12b) is shifted upwards in comparison to the slab track. This fact is due to the reduced stiffness of the ballast track in comparison to the slab track. Thus, this upwards shifts means that the intersection point with the soil dispersion curve will be found on a branch where the shallow layers of the soft soil play a more relevant role. Therefore, a slight increase in the degradation of these layers produces a greater impact, i.e., a greater decrease in the critical speed. This explains the greater influence of the PI on the ballast track critical speed in comparison to the slab track. It should also be highlighted that there is a good fit between the analytical and the numerical results, proving that the region beneath the embankment controls the critical speed of the track. This fact validates the simplification made by the authors in computing the degradation pattern only in the region beneath the embankment.

In order to compare the global degradation levels of both track systems for every PI considered Fig. 13 and Fig. 14 are presented. On scrutinizing the results, it can be seen that for lower PIs a higher degradation is observed, being greater in ballasted track than in slab

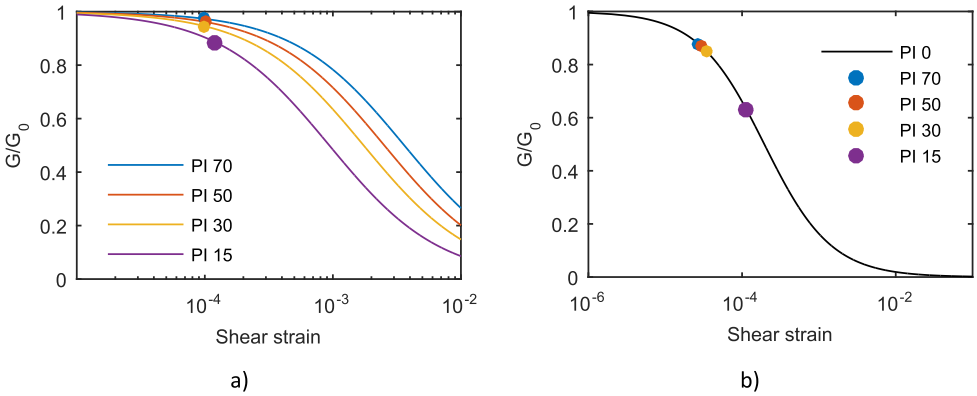

Fig. 16. Average G-degradation in slab track: a) soil; b) embankment.

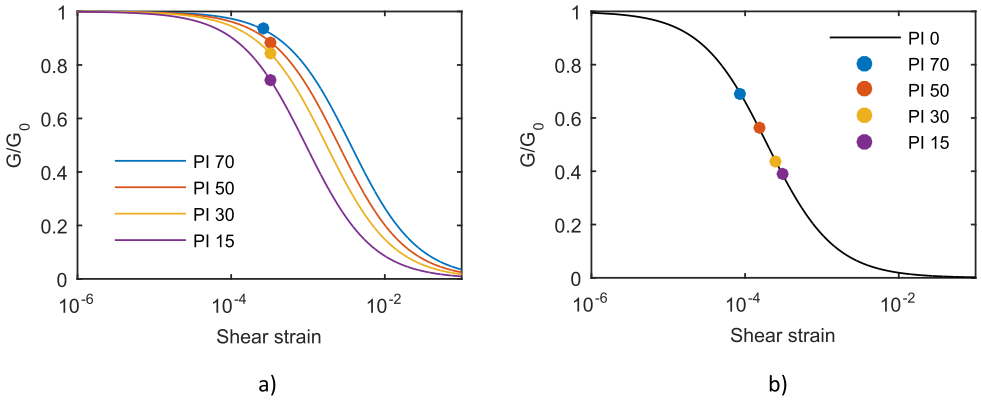

Fig. 17. Average G-degradation in ballasted track: a) soil; b) embankment.

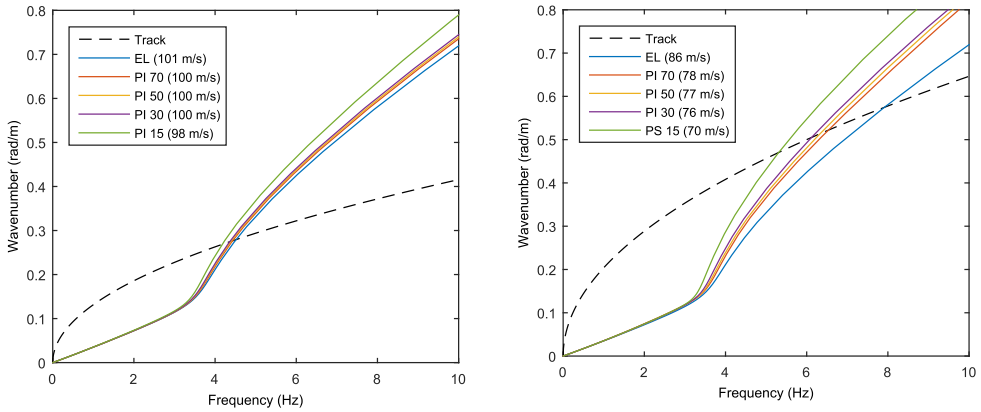

Fig. 18. Dispersion curves for load of 240 kN per bogie: a) slab track; b) ballasted track.

ones. Therefore, it can be seen how lower PIs give rise to lower critical speeds.

4. Influence of axle load

When using a nonlinear constitutive model, the loading magnitude has a major influence once degradation is induced. In this context, the present section assesses the influence of changing the axle load to 120 kN, for all the PI scenarios introduced above, corresponding to the lowest plausible load for a high speed train [17]. The related dynamic amplification curves (DAF) are shown in Fig. 15.

When the results shown in Fig. 15a are compared with the results obtained for an axle load of 180 kN (Fig. 9a), it can be stated the magnitude of axle load has a negligible influence on critical speed for the higher PIs in slab tracks. Conversely, for lower PIs, a small influence can be observed, because a lower load will result in a lower degradation magnitude. For the ballasted track the results for the lightweight axle (Fig. 15b) are compared with those corresponding to the heaviest (Fig. 9b). It is observed that the influence of the magnitude of the load is limited for high values of PI (50–70), hardly varying from 71 m/s to 72 m/s. However, when the PI is low (15–30) the load magnitude for ballasted tracks is influential. More specifically, the critical speed for the lowest PIs is reduced by between 7% and 12%. These differences can be justified that in soils with low PIs the level of degradation is higher, causing a lower critical speed.

As previously described, the degradation pattern is calculated using

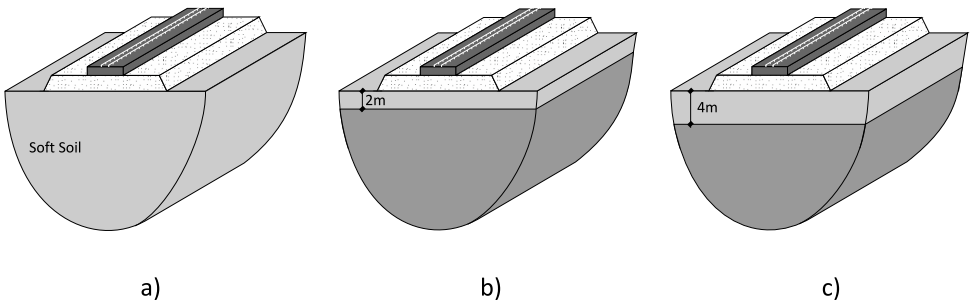

Fig. 19. Variant scenarios: a) Homogeneous; b) 2 m of soft soil; c) 4 m of soft soil.

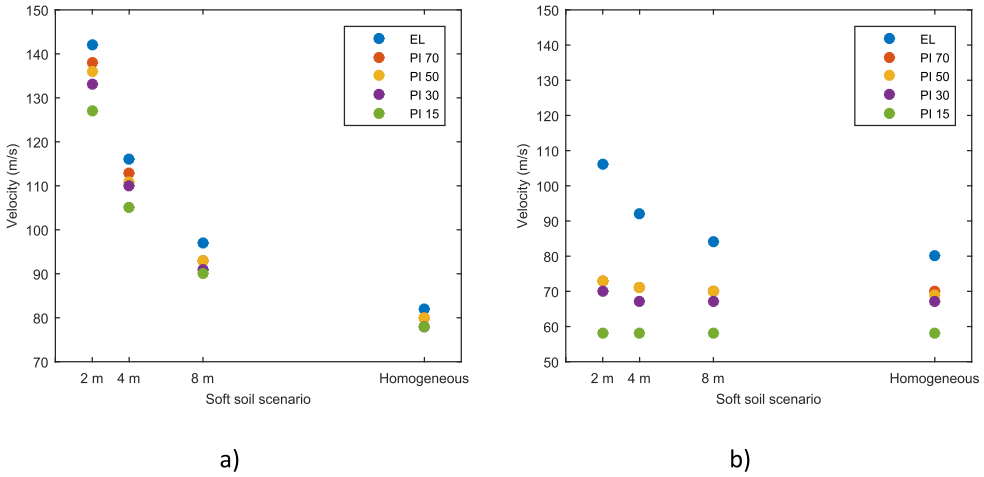

Fig. 20. Critical speed as function of PI and soft soil thickness: a) slab track; b) ballasted track.

Plaxis 3D and the results for the average degradation are shown in Fig. 16 and Fig. 17. As expected, lower degradation percentages are obtained in comparison to the previous cases. Further, for high PI's, the degradation is similar, however for low PI's differences in degradation are more pronounced. This justifies the differences between the critical speeds obtained for the two loading scenarios.

Fig. 18 shows the dispersive analysis for the degraded scenarios. The conclusion drawn for the DAF curves is again true: the critical speeds for the higher PI are almost identical to those expressed in Fig. 12, while the critical speeds are highly sensitive for the lower PI's (30 and 15). Hence, it can be concluded that the loading amplitude has a negligible effect on the critical speed for the case of a slab track, while for ballasted tracks it has a moderate influence on the critical speed for soils with low PIs. However, for soils with high PIs, the effect of the magnitude of the load is practically negligible.

5. Influence of thickness of surface soil layers

To study the influence of surface soil layers, three new scenarios are modelled where the thickness of the top soil layer is either 2 m, 4 m, or infinitely deep, as illustrated in Fig. 19.

For the models presented in Fig. 19, the critical speed for the PI scenarios discussed previously, and the linear elastic case, is calculated. Fig. 20, shows the critical speed for the scenarios, as function of both the PI and upper soil thickness.

From the results, it is observed that the influence of upper soil thickness on critical speed is different for both track systems. Regarding the slab track, for scenarios with thinner upper soil layers, greater dispersion is present when varying the PIs, thus increasing the influence of the (potentially stiffer) soil layers below. Alternatively, for geotechnical profiles with thicker upper soil layers, the effect on critical speed induced by varying PI is residual.

Regarding the ballasted track, the results show that the thickness of the upper soil has limited influence on the critical speed, when considering nonlinearity. This fact is independent of the PI and, for example, comparing the two extreme cases (homogeneous soft soil and soft soil thickness of 2 m) it is observed that both scenarios have a similar critical speed. However, when solely linear elastic behavior is considered, an increase in the thickness of the upper soil layer results in a lower critical speed. Further, the thinner the upper soil layer, the greater the differences between results from the non-linear and the linear elastic models. This occurs because when the upper soil layer is thinner, the increase in stress levels is greater. Therefore, soil strains are greater in a thinner soil layer, causing a greater degradation of the stiffness. This can be seen in Fig. 21, where the shear strains of the two extreme scenarios are compared. Note that in these cases the numerical results are obtained considering linear elastic behavior at the critical speed.

As previously shown in this and other researches [2], the critical speed of ballasted tracks is strongly influenced by the geotechnical characteristics of the shallow soil layers, when considering linear elastic behavior. However, the current analysis shows a weak correlation between the critical velocity and the thickness of the upper soil layer. This is because even for a shallow layer 2 m deep, the stiffer soil below has minimal influence on the critical speed.

In order to confirm this finding, the calculation of the critical speed is carried out for all the scenarios found in Fig. 19 but now considering a shear wave velocity of the upper soil layer of 60 and 100 m/s. The remaining geotechnical properties are identical to those of the reference

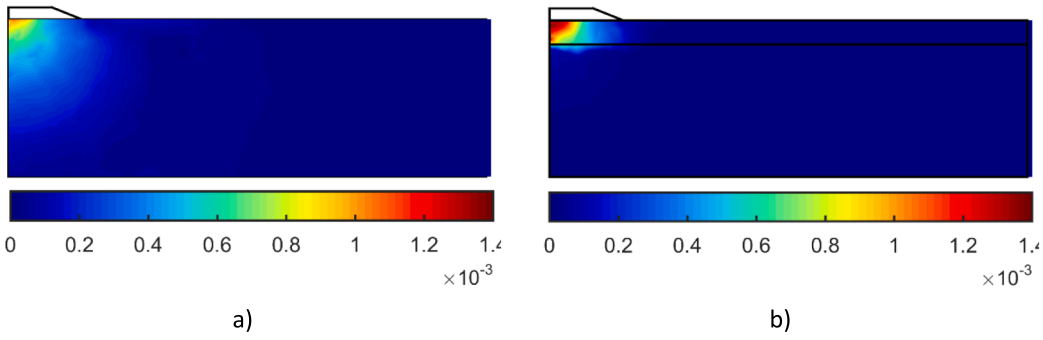

Fig. 21. Shear strain for ballasted track: a) Homogeneous soil; b) Layered with 2 m soft soil.

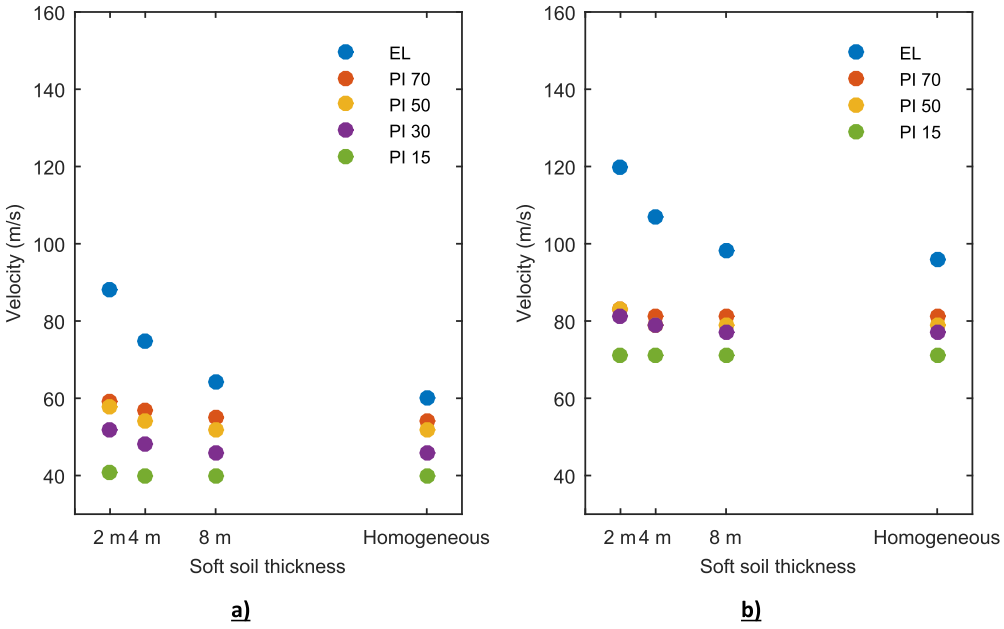

Fig. 22. Critical speed as function of PI and soft soil thickness for: a) Soft soil with C_s of 60 m/s; b) Soft soil with C_s of 100 m/s.

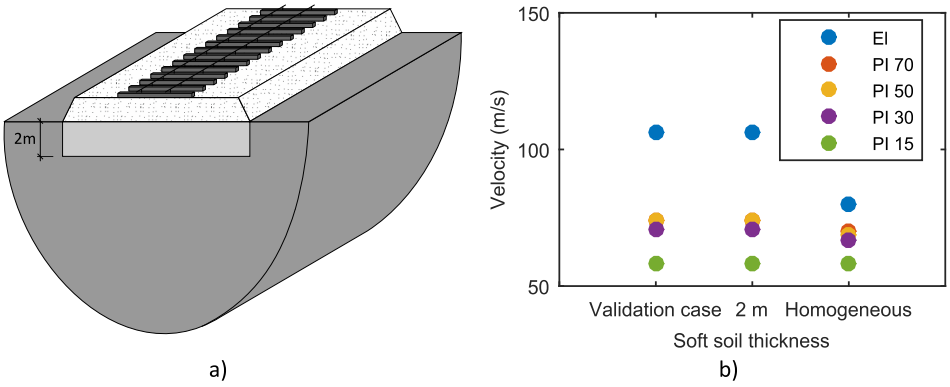

Fig. 23. Test scenario with a thin layer of soft soil: a) 3D scheme; b) Critical speed comparison.

case.

Fig. 22 show the critical speed as a function of the thickness of the upper soil layer and the PI for the two new scenarios. It is seen that the critical speed is almost independent of the thickness of the soil in non-linear models. However, once more, for the linear elastic case an increase in the critical speed is observed as the thickness of the upper soil layer decreases.

Fig. 22a further shows that for the softest soil (C_s = 60 m/s) the thickness of the upper soil layer has a residual influence, which is negligible for the cases of C_s = 80 and 100 m/s. In fact, it can be seen that for thicknesses of 2 m, the critical speed increases slightly compared to the cases of thicknesses 4 m, 8 m and the homogeneous soil in a nonlinear model. This slight increase in critical speed occurs for all PIs except for the lowest (PI 15), for which the critical speed remains unchanged.

To further confirm this finding, one final example is analysed (Fig. 23a), in which the embankment is supported by a thin layer of soft soil (C_s = 80 m/s). Fig. 23b shows the results obtained and they are compared with the reference cases with a thickness of 2 m and the homogeneous soil. As can be seen, the critical speed remains unchanged, verifying that the geotechnical properties of the soft soil on which the track lies are what determines the critical speed.

6. Conclusion

The influence of non-linear soil properties on the track-ground critical speed of high-speed railways has been studied using 3D FEM simulation and analytical dispersion curve analysis.

For slab tracks it has been shown that the effect of non-linear soil behaviour has a moderate influence on the critical speed. For high Plasticity Indexes (PI > 50), the differences with the linear elastic case are below 4% while for low PIs (PI < 30) they are approximately 7%. Thus, a higher PI causes a smaller reduction in the critical speed with respect to the linear elastic case, because the degradation of its stiffness is limited. Further, for the cases studied (axle load <= 180kN), the effect of the magnitude of the load on slab tracks is negligible, causing no notable differences in the critical speed values.

Regarding the influence of the thickness of a soft uppermost soil layer, it has been shown that the effect on slab tracks is important. The greater the thickness of this soft soil, the lower the critical speed,

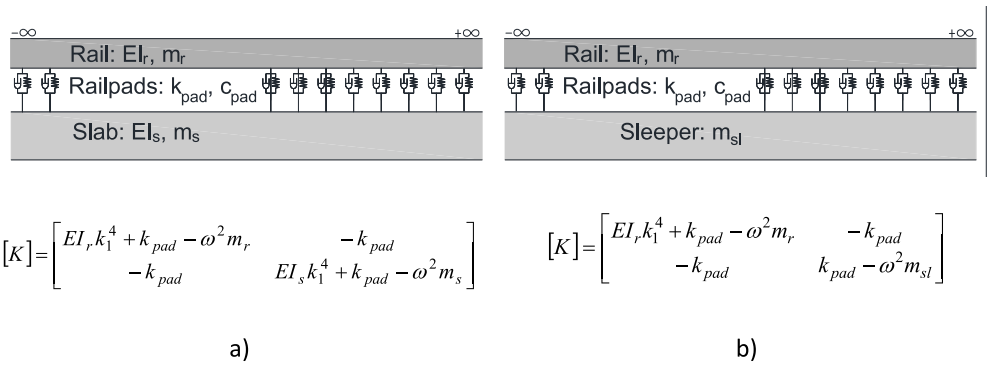

Fig. 24. Analytical description, and corresponding stiffness matrix, of rail tracks adopted in the paper: a) slab track; b) ballast track.

because the deeper stiff soil has a high influence. Regarding the influence of PI, it plays a more important role for thinner layers of soft soil, compared to thicker sections.

For ballast tracks, the critical speed is greatly affected by soil nonlinearity, particularly for lower PI's. In fact, the critical speed for soils with low PI's (IP < 30) is reduced by up to 30% with respect to the linear elastic model, while for high PI's (IP > 50) the maximum difference is 15%. Regarding the influence of the magnitude of the load, it's effect also depends on the PI. For high PI values, the influence of the load magnitude is limited, while for low PIs (15–30) the influence of the load magnitude is higher, reaching differences of up to 12%.

Finally, it has been found that the thickness of upper soft soil layers on ballast tracks has a limited influence on the critical speed, meaning the critical speed is similar for a homogeneous soft soil and a stratum with a thin shallow soft soil layer overlying the same homogenous halfspace. It must be highlighted that such conclusion is related to the scenarios here considered. For these cases, the critical speed is strongly dictated by the characteristics of the soft ground on which the embankment lies.

CRediT authorship contribution statement

Jesus Fernández Ruiz: Conceptualization, Methodology, Writing – original draft, Investigation, Formal analysis, Visualization, Writing – review & editing. **Alexandre Castanheira-Pinto:** Conceptualization, Methodology, Writing – original draft, Investigation, Formal analysis, Visualization, Writing – review & editing. **Pedro Alves Costa:** Conceptualization, Supervision, Writing – review & editing, Resources. **David P. Connolly:** Conceptualization, Supervision, Writing – review & editing, Resources.

Declaration of Competing Interest

The authors declare that they have no known competing financial interests or personal relationships that could have appeared to influence the work reported in this paper.

Acknowledgments

This work was financially supported by: Base Funding - UIDB/04708/2020 and Programmatic Funding - UIDP/04708/2020 of the CONSTRUCT - Instituto de I&D em Estruturas e Construções – funded by national funds through the FCT/MCTES (PIDDAC); Base Funding - UIDB/04029/2020 – of ISISE (Institute for Sustainability and Innovation in Structural Engineering) funded by national funds through the FCT/MCTES (PIDDAC); Project PTDC/ECI-EGC/29577/2017 - POCI-01-0145-FEDER-029577 - and Project PTDC/ECI-EGC/3352/2021, both funded by FEDER funds through COMPETE2020 - Programa Operacional Competitividade e Internacionalização (POCI); National funds (PIDDAC) through FCT/MCTES; Individual Grant: PD/BD/143004/2018 and from the European Union's Horizon 2020 Programme Research and Innovation action under Grant Agreement No 101012456. Funding for open access charge: Universidade da Coruña/CISUG.

Appendix A

Dispersion relation of the ground.

For a ground in free vibration conditions, its dispersive behaviour can be computed by determining the real roots of the dispersion equation. Following the transfer matrix formulation proposed by Sheng et al. [50], the dispersion equation, which establishes a relation between displacements (u_0) and pressures (p_0), is given by:

$$\left([R][S]^{-1}[T_{21}] - [T_{11}]\right)\left\{\widetilde{u}_0\right\} = \left([T_{12}] - [R][S]^{-1}[T_{21}]\right)\left\{\widetilde{p}_0\right\} \tag{A1}$$

In order to obtain non-zero values in the previous equation, the following equation needs to be enforced:

$$\det([K(0,k_3,\omega]) = 0 \tag{A2}$$

where $[K]$ corresponds to the dynamic stiffness matrix:

$$[K(0,k_3,\omega)] = \begin{bmatrix} k_{11}(0,k_3,\omega) & 0 & 0 \\ 0 & k_{22}(0,k_3,\omega) & k_{23}(0,k_3,\omega) \\ 0 & k_{32}(0,k_3,\omega) & k_{33}(0,k_3,\omega) \end{bmatrix} \tag{A3}$$

Thus, for a specific frequencyω, the dispersion curve is obtained by solving the following equation:

$$k_{22}k_{33} - k_{32}k_{23} = 0 \tag{A4}$$

Dispersion relation of the track.

A similar procedure is needed to compute the dispersion curve for a free track in free field condition, where the governing equation is given by:

$$[K]\{u\} = 0 \tag{A5}$$

representing $[K]$ the track's stiffness matrix and $\{u\}$ the vertical displacements.

Assuming a Bernoulli-Euler formulation, both the tracks are modelled as a superposition of Winkler beams as shown in Fig. 24. Superimposed on the Fig. 24 can be found the stiffness matrix for each case.

For a non-zero solution, the determinant of the matrix must respect the following relation:

$$\det([K]) = 0 \tag{A6}$$

Thus, the bending dispersion curve for the track is derived by solving equation (A6).

References

[1] X. Bian, W. Li, J. Hu, H. Liu, X. Duan, Y. Chen, Geodynamics of high-speed railway, Transportation Geotechnics 17 (2018) 69–76.

[2] C. Madshus, S. Lacasse, A. Kaynia, and L. Harvik, "Geodynamic challenges in high speed railway projects," presented at the GeoTrans 2004 - Geotechnical Engineering For Transportation Projects, Los Angeles, 2004.

[3] V.V. Krylov, Generation of ground vibrations by superfast trains, Applied Acoustics 44 (2) (1995) 149–164.

[4] P.A. Costa, A. Colaço, R. Calçada, A.S. Cardoso, Critical speed of railway tracks. Detailed and simplified approaches, Transportation Geotechnics 2 (2015) 30–46.

[5] H.A. Dieterman, A. Metrikine, The equivalent stiffness of a half-space interacting with a beam. Critical velocities of a moving load along the beam, European Journal of Mechanics A/Solids 15 (1) (1996) 67–90.

[6] X. Sheng, C.J.C. Jones, D.J. Thompson, A theoretical study on the influence of the track on train-induced ground vibration, Journal of Sound and Vibration 272 (3–5) (2004) 909–936.

[7] D. Connolly, P.A. Costa, Geodynamics of very high speed transport systems, Soil Dynamics and Earthquake Engineering 130 (2020), 105982.

[8] Y. Gao, H. Huang, C.L. Ho, J.P. Hyslip, High speed railway track dynamic behavior near critical speed, Soil Dynamics and Earthquake Engineering 101 (2017) 285–294.

[9] M. Kaynia, C. Madshus, P. Zackrisson, Ground vibrations from high-speed trains: prediction and countermeasure, Journal of Geotechnical and Geoenvironmental Engineering 126 (6) (2000) 531–537.

[10] C. Madshus, M. Kaynia, High-speed railway lines on soft ground: dynamic behaviour at critical train speed, Journal of Sound and Vibration 231 (3) (2000) 689–701.

[11] A. Karlstrom, B. Bostrom, An analytical model for train-induced ground vibrations from trains, Journal of Sound and Vibration 292 (2006) 221–241.

[12] L. Hall, Simulations and analyses of train-induced ground vibrations in finite element models, Soil Dynamics and Earthquake Engineering 23 (5) (2003) 403–413.

[13] H. Takemiya, Simulation of track–ground vibrations due to a high-speed train: the case of X-2000 at Ledsgard, Journal of Sound and Vibration 261 (3) (2003) 503–526.

[14] P. Alves Costa, R. Calçada, A. Silva Cardoso, A. Bodare, Influence of soil non-linearity on the dynamic response of high-speed railway tracks, Soil Dynamics and Earthquake Engineering 30 (4) (2010) 221–235.

[15] X. Sheng, C.J.C. Jones, M. Petyt, Ground vibration generated by a load moving along a railway track, Journal of Sound and Vibration 228 (1) (1999) 129–156.

[16] F. De Barros, J. Luco, Response of a layered viscoelastic half-space to a moving point load, Wave motion 19 (2) (1994) 189–210.

[17] A. Colaço, P.A. Costa, D.P. Connolly, The influence of train properties on railway ground vibrations, Structure and Infrastructure Engineering 12 (5) (2016) 517–534.

[18] P. Galvín, D.L. Mendoza, D.P. Connolly, G. Degrande, G. Lombaert, A. Romero, Scoping assessment of free-field vibrations due to railway traffic, Soil Dynamics and Earthquake Engineering 114 (2018) 598–614.

[19] S. François, M. Schevenels, P. Galvín, G. Lombaert, G. Degrande, A 2.5D coupled FE–BE methodology for the dynamic interaction between longitudinally invariant structures and a layered halfspace, Computer Methods in Applied Mechanics and Engineering 199 (23–24) (2010) 1536–1548.

[20] P. Galvín, S. François, M. Schevenels, E. Bongini, G. Degrande, G. Lombaert, A 2.5D coupled FE-BE model for the prediction of railway induced vibrations, Soil Dynamics and Earthquake Engineering 30 (12) (2010) 1500–1512.

[21] H. Chebli, D. Clouteau, L. Schmitt, Dynamic response of high-speed ballasted railway tracks: 3D periodic model and in situ measurements, Soil Dynamics and Earthquake Engineering 28 (2) (2008) 118–131.

[22] H. Chebli, R. Othman, D. Clouteau, M. Arnst, G. Degrande, 3D periodic BE-FE model for various transportation structures interacting with soil, Computes and Geotechnics 35 (1) (2008) 22–32.

[23] D.P. Connolly, K. Dong, P. Alves Costa, P. Soares, P.K. Woodward, "High speed railway ground dynamics: a multi-model analysis," *International Journal of Rail,* Transportation 8 (4) (2020) 324–346.

[24] Y.B. Yang, H.H. Hung, D.W. Chang, Train-induced wave propagation in layered soils using finite/infinite element simulation, Soil Dynamics and Earthquake Engineering 23 (4) (2003) 263–278.

[25] P. Galvín, A. Romero, and J. Domínguez, "Fully three-dimensional analysis of high-speed train–track–soil-structure dynamic interaction," *Journal of Sound and Vibration,* vol. 329, no. 24, pp. 5147-5163, 11/22/ 2010.

[26] J. O'Brien, D.C. Rizos, A 3D BEM-FEM methodology for simulation of high speed train induced vibrations, Soil Dynamics and Earthquake Engineering 25 (4) (2005) 289–301.

[27] J.-Y. Shih, D.J. Thompson, A. Zervos, The influence of soil nonlinear properties on the track/ground vibration induced by trains running on soft ground, Transportation Geotechnics 11 (2017) 1–16.

[28] M.A. Sayeed, M.A. Shahin, Three-dimensional numerical modelling of ballasted railway track foundations for high-speed trains with special reference to critical speed, Transportation Geotechnics 6 (2016) 55–65.

[29] A. El Kacimi, P.K. Woodward, O. Laghrouche, G. Medero, Time domain 3D finite element modelling of train-induced vibration at high speed, Computers & Structures 118 (2013) 66–73.

[30] J. Chen, Y. Zhou, Dynamic responses of subgrade under double-line high-speed railway, Soil Dynamics and Earthquake Engineering 110 (2018) 1–12.

[31] J. Fernández-Ruiz, M. Miranda, J. Castro, L.M. Rodríguez, Improvement of the critical speed in high-speed ballasted railway tracks with stone columns: A numerical study on critical length, Transportation Geotechnics 30 (2021), 100628.

[32] L. Hall, "Simulations and Analyses of Train-Induced Ground Vibrations. A comparative study of two- and three-dimensional calculations with actual measurements," PhD thesis, Division of Soil and Rock Mechanics, Royal Institute of Technology (KTH), Stockholm, 2000.

[33] K. Dong, D. Connolly, O. Laghrouche, P. Woodward, P.A. Costa, Non-linear soil behaviour on high speed rail lines, Computers and Geotechnics 112 (2019) 302–318.

[34] S. Kramer, Geotechnical earthquake engineering, Prentice-Hall, New Jersey, 1996.

[35] B. Hardin, V. Drnevich, Shear Modulus and Damping in Soils: Measurement and Parameter Effects (Terzaghi Lecture), Journal of the Soil Mechanics and Foundation Division 98 (6) (1972) 603–624.

[36] B. Hardin, V. Drnevich, Shear modulus and damping in soils: design equations and curves, Journal of the Soil Mechanics and Foundation Division 98 (7) (1972) 667–692.

[37] M. Vucetic, R. Dobry, Effect of soil plasticity on cyclic response, Journal of Geotechnical Engineering Division 117 (1991) 89–117.

[38] I. Ishibashi, X. Zhang, Unified dynamic shear moduli and damping ratios of sand and clay, Soils and Foundations 33 (1) (1993) 182–191.

[39] R. B. J. K. Brinkgreve, S.; Swolfs, W.M.; Zampich, L.; Ragi Manoj, N., *Plaxis 2019 User Manuals*. Delft, 2019.

[40] J. Fernández Ruiz, P. Alves Costa, R. Calçada, L. E. Medina Rodríguez, and A. Colaço, "Study of ground vibrations induced by railway traffic in a 3D FEM model formulated in the time domain: experimental validation," *Structure and Infrastructure Engineering,* pp. 1-13, 2017.

[41] J. Fernández-Ruiz, L.E.M. Rodríguez, P.A. Costa, M. Martínez-Díaz, Benchmarking of two three-dimensional numerical models in time/space domain to predict railway-induced ground vibrations, Earthquake Engineering and Engineering Vibration 20 (1) (2021) 245–256.

[42] J. Fernández-Ruiz, L.E. Medina Rodríguez, P.A. Costa, Use of Tyre-Derived Aggregate as Backfill Material for Wave Barriers to Mitigate Railway-Induced Ground Vibrations, International Journal of Environmental Research and Public Health 17 (24) (2020) 9191.

[43] V. Galavi, R. Brinkgreve, Finite element modelling of geotechnical structures subjected to moving loads, VIII ECNUMGE-Numerical Methods in Geotechnical Engineering 1 (2014) 235–240.

[44] T. Benz, Small-strain stiffness of soils and its numerical consequences, Institut für Geotechnik der Universität Stuttgart, PhD, 2006.

[45] J.F. Ruiz, P.J. Soares, P.A. Costa, D.P. Connolly, The effect of tunnel construction on future underground railway vibrations, Soil Dynamics and Earthquake Engineering 125 (2019), 105756.

[46] R. Brinkgreve, M. Kappert, and P. Bonnier, "Hysteretic damping in a small-strain stiffness model," *Proc. of Num. Mod. in Geomech., NUMOG X, Rhodes,* pp. 737-742, 2007.

[47] J. L. L'Heureux, M., "Correlations between shear wave velocity and geotechnical parameters in Norwegian clays," Norwegian Geotechnical Institute2015.

[48] A. Castanheira-Pinto, A. Colaço, J. F. Ruiz, P. A. Costa, and L. Godinho, "Simplified approach for ground reinforcement design to enhance critical speed," *Soil Dynamics and Earthquake Engineering*, Article vol. 153, 2022, Art. no. 107078.
[49] P.A. Costa, P. Soares, A. Colaço, P. Lopes, D. Connolly, Railway critical speed assessment: A simple experimental-analytical approach, Soil Dynamics and Earthquake Engineering 134 (2020), 106156.
[50] X. Sheng, C. Jones, D. Thompson, A theoretical study on the influence of the track on train-induced ground vibration, Journal of Sound and Vibration 272 (2004) 909–936.